RKKY interaction in graphene bubbles

Binyuan Zhang, Liwei Jiang,* and Yisong Zheng*

Key Laboratory of Physics and Technology for Advanced Batteries (Ministry of Education), Department of Physics, Jilin University, Changchun 130012, China

(Received 2 February 2019; revised manuscript received 3 April 2019; published 17 June 2019)

By means of the Lanczos method, a numerically efficient theoretical approach, we study the Ruderman-Kittel-Kasuya-Yosida (RKKY) interaction in a graphene bubble. We find that the RKKY interaction in a graphene bubble can be larger or smaller than the corresponding result in pristine graphene by a few orders of magnitude, depending on the sublattice attribution and pseudomagnetic field strength where two magnetic impurities are positioned, which is due to the sublattice polarization of the low-energy electronic states in a strong pseudomagnetic field. If two magnetic impurities are both in the bubble region, the R^{-3} decay rate of the RKKY interaction found in pristine graphene breaks down. But it recovers when one magnetic impurity is far away from the bubble center no matter where another impurity is located. When the Fermi level deviates from the Dirac point by carrier doping, the antiferromagnetic RKKY interaction between two magnetic impurities located at the opposite sublattices can be inverted to be ferromagnetic by altering the bubble height properly.

DOI: 10.1103/PhysRevB.99.245410

I. INTRODUCTION

Graphene is a two-dimensional topological Dirac semimetal; hence, it possesses some novel electronic properties [1–10], such as Ruderman-Kittel-Kasuya-Yosida (RKKY) interaction, different from conventional two-dimensional materials. The RKKY interaction is an indirect exchange interaction between two magnetic impurities mediated by the conduction electrons of the host material such as graphene [11–13]. In charge-neutral graphene, the RKKY interaction obeys the so-called Saremi's rule. Namely, it is ferromagnetic between magnetic impurities located on the same sublattice but antiferromagnetic between impurities located on opposite sublattices [14–16]. Furthermore, with the increase of the distance between two magnetic impurities R, the RKKY interaction in graphene decays as R^{-3}, rather than R^{-2} in the conventional two-dimensional materials [16–19].

As a convenient experimental measure to modulate the low-energy electronic properties around the Dirac point, strain in graphene has drawn much attention in both theoretical and experimental studies. A critical strain effect on the electron states in graphene is that it can induce a huge out-of-plane pseudomagnetic field [20,21]. And different strain fields may induce different pseudomagnetic fields [22,23]. Unlike a realistic magnetic field, the so-called pseudomagnetic field has just a sign inversion when it acts on the K and K' valley electrons. Experimentally, strain always exists along with graphene bubbles where lattice deformation inevitably appears. It was observed that bubbles form frequently when graphene grows on and couples to the substrate. For example, graphene nanobubbles can be observed when mechanically exfoliated graphene is mounted on a SiO_2/Si substrate and subjected to HF/H_2O etching or irradiation by energetic protons [24]. Recently, it became possible to control the curvature of a spherical graphene bubble by applying an electric field [25]. This paves the way to explore the Dirac fermion property in the case of a strong and tunable magnetic field. It was reported that the strength of the strain-induced pseudomagnetic field can be greater than 300 T in a graphene nanobubble, which results in discrete pseudo-Landau levels in the band structure of graphene [26]. Recent theoretical studies indicated the local density of states in a graphene bubble exhibits a sixfold symmetry pattern, with sublattice polarization in each sector. Electrons are well confined in the armchair directions, while the zigzag directions allow the flow of probability current between the inside and outside of the strained region. In addition, because the direction of a pseudomagnetic field switches between the inequivalent Dirac valleys [20,27], the graphene nanobubble is considered a device prototype to realize both the valley filtering and valley splitting functions [28].

Owing to the presence of induced pseudomagnetic magnetic field, the RKKY interaction in a graphene bubble is expected to present different behaviors in comparison with the case in pristine graphene. On the one hand, from the aspect of fundamental physics, whether the R^{-3} decay rate and Saremi's rule hold true for the RKKY interaction in a graphene bubble needs to be reexamined. On the other hand, the tunable size of the bubble provides us with the possibility to control the RKKY interaction in a graphene bubble, which is significant for the purposes of manipulating the spin to realize device functions in dilute magnetic impurity-doped graphene bubbles. However, the theoretical study of the RKKY interaction in a graphene bubble is very difficult because the existence of a bubble breaks the periodicity of pristine graphene; hence, the electronic states of such a system are hard to solve. In this paper, we adopt the Lanczos method in real lattice space, which has no need for artificial finite boundaries or periodic

*Corresponding author: zhengys@jlu.edu.cn

conditions of the system to investigate the RKKY interaction in the graphene bubble. Therefore, it is a numerically efficient theoretical approach. We find that in comparison with the case in pristine graphene, the RKKY interaction in a graphene bubble exhibits sizable variation. It can be larger or smaller than the corresponding result in pristine graphene by a few orders of magnitude, depending on the sublattice attribution and pseudomagnetic field strength where two magnetic impurities are positioned. This arises from the sublattice polarization of the low-energy electronic states induced by the strong pseudomagnetic field. If the magnetic impurities are both in the bubble region, the R^{-3} decay rate breaks down. But it recovers when one magnetic impurity is far away from the bubble center no matter where another impurity is located in. When the Fermi level deviates from the Dirac point by carrier doping, the antiferromagnetic coupling between two magnetic impurities located at opposite sublattices can be inverted to be ferromagnetic by altering the bubble height.

This paper is organized as follows. In Sec. II, the shape and corresponding tight-binding Hamiltonian of the graphene bubble are introduced, and then the Lanczos method we use to obtain the retarded Green's function and furthermore to calculate the RKKY interaction is presented. In Sec. III, the numerical results of the RKKY interaction in a graphene bubble are shown and discussed. Finally, in Sec. IV the main results are summarized briefly.

II. METHODS

As shown in Fig. 1(a), the carbon atoms in a bubble rise from the otherwise planar graphene lattice. Without loss of generality, we adopt a Gaussian function $z(r) = h\exp(-r^2/2\sigma^2)$ to measure the out-of-plane displacement of carbon atoms from the lattice plane of pristine graphene, with h and σ characterizing the height and width of the bubble, respectively [28–30]. And $r = \sqrt{x^2 + y^2}$ is the in-plane coordinate of a carbon atom which is assume to be unaffected by the presence of the bubble for simplicity. Accordingly, the carbon-carbon bonds in the bubble region are inevitably stretched, which could modify the hopping parameter in the electronic tight-binding model. Within the nearest-neighbor approximation, the tight-binding Hamiltonian of graphene even in the presence of a bubble is formally written as

$$\hat{H} = \sum_{\langle l j\alpha, l' j'\alpha'\rangle} t_{l j\alpha, l' j'\alpha'} |l j\alpha\rangle\langle l' j'\alpha'| + \text{H.c.}, \tag{1}$$

where $|l j\alpha\rangle$ stands for the atomic orbit of the π-band electron of graphene. l and j are integers, and $\alpha = A/B$ labels the inequivalent carbons in the A/B sublattices. The indexes $(l j\alpha)$ can fully determine the in-plane coordinate of a carbon atom as $\mathbf{r}_{l j\alpha} = l\mathbf{a}_1 + j\mathbf{a}_2 + \boldsymbol{\tau}_\alpha$, with $\mathbf{a}_1 = a/2(-\sqrt{3}, 3, 0)$ and $\mathbf{a}_2 = a/2(-\sqrt{3}, -3, 0)$. As shown in Fig. 1(b), they are the primitive lattice vectors, with a being the C-C bond length of the pristine graphene (hereafter we set $a = 1$ as the unit of length). In addition, $\boldsymbol{\tau}_A = (0, -1/2, 0)$ and $\boldsymbol{\tau}_B = (0, 1/2, 0)$ identify the positions of A and B atoms in a unit cell, respectively. Then, the z coordinate of an atom in a Gaussian bubble is given by $z(r_{l j\alpha})$. In the Hamiltonian the notation $\langle l j\alpha, l' j'\alpha'\rangle$ means that the summation is restricted

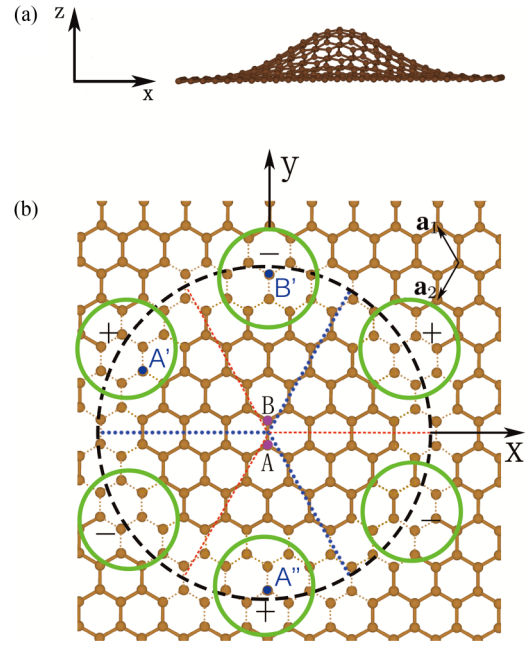

FIG. 1. (a) The side view and (b) top view of a Gaussian graphene bubble with the center at the origin of Cartesian coordinates. In (b) $\mathbf{a}_1$ and $\mathbf{a}_2$ are the primitive lattice vectors of pristine graphene. The large dashed circle denotes the contour of the half height of the bubble ($r = \sigma$). The spatially nonuniform pseudomagnetic field in the bubble has threefold rotational symmetry. The six small solid circles specify the maximal pseudomagnetic field regions, with + and − signs denoting the pseudomagnetic field in the $\pm z$ directions, respectively. Points A, A', A'', B, and B' denote the typical positions of the magnetic field to calculate the RKKY interactions.

within the nearest-neighbor atomic pairs, with $t_{l j\alpha, l' j'\alpha'}$ being the corresponding hopping parameter. In the presence of the bubble, $t_{l j\alpha, l' j'\alpha'}$ is a function of local bond length of the nearest-neighbor atomic pairs

$$t_{l j\alpha, l' j'\alpha'} = t\exp\{-3.37[|z(r_{l j\alpha}) - z(r_{l' j'\alpha'})|^2 + 1]^{1/2} - 1\}, \tag{2}$$

where t is the nearest-neighbor hopping parameter of pristine graphene [31]. We use it as the unit of energy in the numerical calculations.

Following the original RKKY theory, two magnetic impurities, $\hat{\mathbf{S}}_1$ and $\hat{\mathbf{S}}_2$, settled on the lattice points (l, j, α) and (l', j', α'), respectively, can establish an indirect exchange interaction mediated by the conduction electrons of graphene even in the presence of a bubble,

$$\hat{H}_{RKKY} = J_{\alpha,\alpha'}(l j, l' j')\hat{\mathbf{S}}_1 \cdot \hat{\mathbf{S}}_2. \tag{3}$$

The RKKY interaction is defined as [16,32]

$$J_{\alpha,\alpha'}(l j, l' j') = -\frac{\hbar^2 J^2}{2\pi}\int_{-\infty}^{E_F} d\varepsilon \,\mathrm{Im}\big[G^r_{l j\alpha, l' j'\alpha'}(\varepsilon) G^r_{l' j'\alpha', l j\alpha}(\varepsilon)\big], \tag{4}$$

where J denotes the exchange energy between the magnetic impurity and the carbon atom it sits right on. E_F is the Fermi energy of the graphene bubble. In the above equation, $G^r_{l j\alpha, l' j'\alpha'}$ is the retarded lattice Green's function. We must

point out that the RKKY interaction defined herein is only a single-particle approximation of a many-body problem which includes the interaction between the local magnetic moment and conduction electrons. It is only suitable for the case of weak coupling between the local magnetic moment and the spin of the conduction electron. In terms of the eigenexpansion of the Green's function and via a straightforward derivation we can obtain an alternative expression of the RKKY interaction which is helpful for us to understand the numerical result of the RKKY interaction shown below. It is given by

$$\begin{aligned} J_{\alpha,\alpha'}(l\,j,l'\,j') = \hbar^2 J^2 \mathrm{Re}[&\langle l\,j\alpha|\psi_m\rangle\langle\psi_m|l'\,j'\alpha'\rangle \\ &\times \langle l'\,j'\alpha'|\psi_n\rangle\langle\psi_n|l\,j\alpha\rangle] \\ &\times \sum_{m,n} \frac{\theta(E_F - E_n)\theta(E_m - E_F)}{E_n - E_m}, \end{aligned} \tag{5}$$

where $|\psi_i\rangle$ and E_i represent, respectively, the eigenstate and the corresponding energy of graphene with a bubble, although it is rather difficult to get the complete set of them. $\theta(x)$ is the conventional step function. From such an expression one can readily infer that the RKKY interaction is mainly determined by the occupied and unoccupied states near the Fermi level.

As seen from Eq. (4), the retarded Green's function between the two lattice points where the magnetic impurities are positioned is the critical quantity for us to work out the RKKY interaction. However, due to the presence of the bubble it is a rather tough task to get such a Green's function. In this work we employ the Lanczos method in real space with which we can get the numerical Green's function [33]. The key procedure of such a method is to find out a basis set in which the tight-binding Hamiltonian of a graphene bubble becomes a tridiagonal matrix. In so doing, we first choose a normalized seed state $|f_0\rangle$, then construct a new state orthogonal to $|f_0\rangle$ using the following formulas:

$$|F_1\rangle = \hat{H}|f_0\rangle - |f_0\rangle\langle f_0|\hat{H}|f_0\rangle = \hat{H}|f_0\rangle - a_0|f_0\rangle, \tag{6}$$

$$|f_1\rangle = \frac{1}{b_1}|F_1\rangle, \tag{7}$$

where $a_0 = \langle f_0|\hat{H}|f_0\rangle$ and $b_1 = \langle f_0|\hat{H}|f_1\rangle$ is the normalization coefficient of state $|f_1\rangle$. Apparently, $|f_1\rangle$ is orthogonal to $|f_0\rangle$. It is easy to get the recursive relation when $n \geqslant 2$,

$$|F_n\rangle = \hat{H}|f_{n-1}\rangle - a_{n-1}|f_{n-1}\rangle - b_{n-1}|f_{n-2}\rangle, \tag{8}$$

$$|f_n\rangle = \frac{1}{b_n}|F_n\rangle, \tag{9}$$

with the recursive coefficients

$$a_n = \langle f_n|\hat{H}|f_n\rangle, \tag{10}$$

$$b_n = \langle f_{n-1}|\hat{H}|f_n\rangle. \tag{11}$$

We can prove that every new state obtained with Eqs. (8) and (9) is normalized and they are orthogonal to each other.

On the basis of $\{|f_0\rangle, |f_1\rangle, |f_2\rangle, \ldots\}$ the tight-binding Hamiltonian of the graphene bubble becomes a tridiagonal matrix which takes the form

$$H = \begin{bmatrix} a_0 & b_1 & 0 & \cdots \\ b_1 & a_1 & b_2 & \cdots \\ 0 & b_2 & a_2 & \ddots \\ \vdots & \vdots & \ddots & \ddots \end{bmatrix}. \tag{12}$$

Since the retarded Green's function matrix is defined as $\hat{G}^r(\varepsilon) = (\varepsilon - \hat{H} + i\eta)^{-1}$, with η being the infinitesimal, the first diagonal element of such a Green's function can be written as

$$G^r_{00}(\varepsilon) = \langle f_0|\hat{G}^r(\varepsilon)|f_0\rangle = \frac{D_1}{D}, \tag{13}$$

where D is the determinant of the matrix $[\varepsilon - H + i\eta]$. D_i for $i \geqslant 1$ is the determinant of the matrix by taking out both the first i rows and first i columns of $[\varepsilon - H + i\eta]$. We can expand D by using Laplace's theorem,

$$D = (\varepsilon + i\eta - a_0)D_1 - b_1^2 D_2, \tag{14}$$

so we can express $G^r_{00}(\varepsilon)$ as

$$G^r_{00}(\varepsilon) = \frac{1}{\varepsilon + i\eta - a_0 - b_1^2 \frac{D_2}{D_1}}. \tag{15}$$

Analogously, D_i can be expanded by D_{i+1} and D_{i+2} as

$$D_i = (\varepsilon + i\eta - a_i)D_{i+1} - b_{i+1}^2 D_{i+2}. \tag{16}$$

Then we can get $G^r_{00}(\varepsilon)$ by using the continued fraction expansion method. In the actual calculation, we can take a cutoff of the tridiagonal Hamiltonian matrix as long as the retarded Green's function is converged. Namely, a_∞ and b_∞ are terminated at a_N and b_N, respectively. Then

$$G^r_{00}(\varepsilon) = \cfrac{1}{\varepsilon + i\eta - a_0 - \cfrac{b_1^2}{\varepsilon + i\eta - a_1 - \cfrac{b_2^2}{\varepsilon + i\eta - a_2 - \cdots - b_{N-1}^2 \Sigma(\varepsilon)}}}, \tag{17}$$

where

$$\Sigma(\varepsilon) = \frac{\varepsilon - i\sqrt{4b_N^2 - (\eta - a_N)^2} - a_N}{2b_N^2}. \tag{18}$$

If we construct the seed state in the manner $|f_0\rangle = c_1|l\,j\alpha\rangle + c_2|l'\,j'\alpha'\rangle$, with c_1 and c_2 being the arbitrary normalized coefficients, the obtained Green's function $G^r_{00}(\varepsilon)$ is associated with the ones used in Eq. (4), i.e.,

$$\begin{aligned} G^r_{00}(\varepsilon) = |c_1|^2 G^r_{l\,j\alpha,l\,j\alpha}(\varepsilon) + |c_2|^2 G^r_{l'\,j'\alpha',l'\,j'\alpha'}(\varepsilon) \\ + c_1^* c_2 G^r_{l\,j\alpha,l'\,j'\alpha'}(\varepsilon) + c_1 c_2^* G^r_{l'\,j'\alpha',l\,j\alpha}(\varepsilon). \end{aligned} \tag{19}$$

Then, by altering the normalized coefficients and repeating the above Lanczos procedure, we can finally obtain the Green's functions $G^r_{l\,j\alpha,l'\,j'\alpha'}(\varepsilon)$ and $G^r_{l'\,j'\alpha',l\,j\alpha}(\varepsilon)$ essential for calculating the RKKY interaction by using Eq. (4). In the numerical calculations, we set $\eta = 0.001|t|$, and we find that the recursive number $N = 3000$ is sufficient to result in a converged result.

III. NUMERICAL RESULTS

A. Pristine graphene

By means of the theoretical method presented above, we are now ready to calculate the RKKY interaction in graphene. First of all, it is significant to use the Lanczos method outlined above to study the RKKY interaction in pristine graphene. By comparison with the relevant results in previous studies, the validity of the Lanczos method can be checked. As a comparative study, in addition to the Lanczos method, we also adopt the eigenfunction expansion method to obtain the retarded lattice Green's function of pristine graphene, with which the RKKY interaction of pristine graphene can then be calculated. The main steps to get the Green's function using the eigenfunction expansion method are as follows. First, the electronic eigenfunction of pristine graphene within the tight-binding model is given by

$$\psi^{\pm}_{\mathbf{k}}(\mathbf{r}) = \sqrt{\frac{1}{N}} \sum_{l,j} [c^{\pm}_{A}(\mathbf{k}) e^{i\mathbf{k}\cdot\mathbf{r}_{ljA}} |l\,jA\rangle + c^{\pm}_{B}(\mathbf{k}) e^{i\mathbf{k}\cdot\mathbf{r}_{ljB}} |l\,jB\rangle], \tag{20}$$

with the coefficient

$$c^{\pm}_{A}(\mathbf{k}) = \frac{1 + e^{iak_y} + e^{i\frac{\sqrt{3}ak_x + ak_y}{2}}}{\left(2 + 8cos^2\frac{aky}{2} + 8cos\frac{aky}{2}cos\frac{\sqrt{3}akx}{2}\right)^{\frac{1}{2}}}, \tag{21}$$

$$c^{\pm}_{B}(\mathbf{k}) = \pm\frac{1}{\sqrt{2}}, \tag{22}$$

and the corresponding eigenenergies are

$$E_{\pm}(\mathbf{k}) = \pm\left(1 + 4\cos^2\frac{aky}{2} + 4\cos\frac{aky}{2}\cos\frac{\sqrt{3}akx}{2}\right)^{\frac{1}{2}}, \tag{23}$$

where $\pm$ stands for the conduction band and valence band, respectively. Then, by expanding the Green's function $\hat{G}^r = (\varepsilon - \hat{H} + i\eta)^{-1}$ in the eigenrepresentation, we can readily obtain the retarded lattice Green's function used to calculate RKKY interaction, which can be expressed as

$$G^r_{lj\alpha,l'j'\alpha'}(\varepsilon) = \sum_{\mathbf{k}} \left[\frac{c^{+}_{\alpha}(\mathbf{k})^*\, c^{+}_{\alpha'}(\mathbf{k})\, e^{i\mathbf{k}\cdot(\mathbf{r}_{l'j'\alpha'} - \mathbf{r}_{lj\alpha})}}{\varepsilon - E_{+} + i\eta} + \frac{c^{-}_{\alpha}(\mathbf{k})^*\, c^{-}_{\alpha'}(\mathbf{k})\, e^{i\mathbf{k}\cdot(\mathbf{r}_{l'j'\alpha'} - \mathbf{r}_{lj\alpha})}}{\varepsilon - E_{-} + i\eta} \right], \tag{24}$$

where the $\mathbf{k}$ summation is taken over the whole Brillouin zone.

The numerical results of RKKY interaction of pristine graphene with the lattice Green's functions calculated by the Lanczos and eigenfunction expansion methods are shown in Fig. 2. We plot $J_{AA}(\boldsymbol{R})$ and $J_{AB}(\boldsymbol{R})$ as a function of $R = |\boldsymbol{R}|$, with $\boldsymbol{R} = \boldsymbol{r}_{lj\alpha} - \boldsymbol{r}_{l'j'\alpha'}$ being the distance between the two magnetic impurities. We can see that the results of the two methods are consistent with each other without a discernible difference in the total range of $|R|$. However, the computation of the lattice Green's function using the eigenfunction expansion method is rather time-consuming, in contrast to the Lanczos method. This is due to the fact that a very fine $\boldsymbol{k}$ mesh is required to get a convergent result of the lattice Green's function as shown in Eq. (24). From the results shown in Fig. 2, we can see that with the increase of R, the RKKY interaction follows a R^{-3} decay rate for both cases of $\boldsymbol{R}$ going along the armchair and zigzag directions. But in zigzag direction the RKKY interaction shows a periodic oscillation. Moreover, the RKKY interaction of pristine graphene is ferromagnetic (antiferromagnetic) if the carbon atoms under two magnetic impurities belong to the same sublattice (distinct sublattices). All of these features of RKKY interaction of pristine graphene which we get via the Lanczos method have been reported in previous studies [34,35]. But an advantage of the Lanczos method is that it can be used to study the RKKY interaction in graphene even without the lattice periodicity, e.g., the graphene bubble.

B. Graphene bubble

In this section we turn to consider the RKKY interaction in a graphene bubble. Our aim is to uncover the novel features of the RKKY interaction in graphene brought about by the presence of a bubble. In a graphene bubble the lattice deformation brings about a pseudomagnetic field; hence, the RKKY interaction in it is expected to be more complicated.

To study numerically the RKKY interaction we assume that the graphene bubble is charge neutral unless otherwise specified. In so doing, we set the Fermi energy at the Dirac point, i.e., $E_F = 0$. According to the relevant literature, we choose the size of a typical bubble to be $h = 3.5$ nm and $\sigma = 5$ nm [28]. In this context, the most stretched nearest-neighbor C-C bond length around the half height ($r = \sigma$) of the bubble is enhanced by about 8.5%, which is far lower than the elastic tensile limit (25%)[36]. Due to the breakdown of the lattice translation symmetry, unlike the case in pristine graphene, the RKKY interaction in a graphene bubble depends on not only R but also the respective positions of the two magnetic impurities with respect to the bubble center. Therefore, to study the RKKY interaction in a graphene bubble, first of all, we need to specify one magnetic impurity somewhere. To begin with, we consider the cases in which one impurity, say, $(l\,j\alpha)$, is fixed at $(0, 0, A)$ or $(0, 0, B)$, closest to the bubble center, as shown in Fig. 1(b), while the position of another impurity, $(l'\,j'\alpha')$, is altered along the armchair line, i.e., the y axis. Thus, the RKKY interactions for these cases in a graphene bubble are functions of $\boldsymbol{R} = \boldsymbol{r}_{\alpha l j} - \boldsymbol{r}_{\alpha' l' j'}$. And they are different from each other owing to the different positions of the fixed impurity. Below we will use the shorthand $J_{\alpha,\alpha'}(\boldsymbol{R})$ for the RKKY interaction for compactness. From the numerical results shown in Fig. 3(a) we can see that $J_{AA}(\boldsymbol{R})$ is always identical to $J_{BB}(-\boldsymbol{R})$. Guided by the lattice schematic shown in Fig. 1(b), we can readily understand that this is a straightforward result of spatial inversion symmetry of a graphene bubble.

It is evident that none of the $J_{\alpha\alpha}(\boldsymbol{R})$'s in the graphene bubble shown in Fig. 3(a) show any nontrivial difference from the one in pristine graphene in the small-R limit ($R < 12a$). However, when R is in a moderate region ($12a \leqslant R < 60a$), $J_{AA}(\boldsymbol{R} < 0)$ is much larger, but $J_{AA}(\boldsymbol{R} > 0)$ is much smaller than its counterpart in pristine graphene. For example, as shown in Fig. 3(a), at $R = 45a$ the former is larger, and at $R = 60a$ the latter is smaller than the corresponding values of the RKKY interaction in pristine graphene by one and two orders

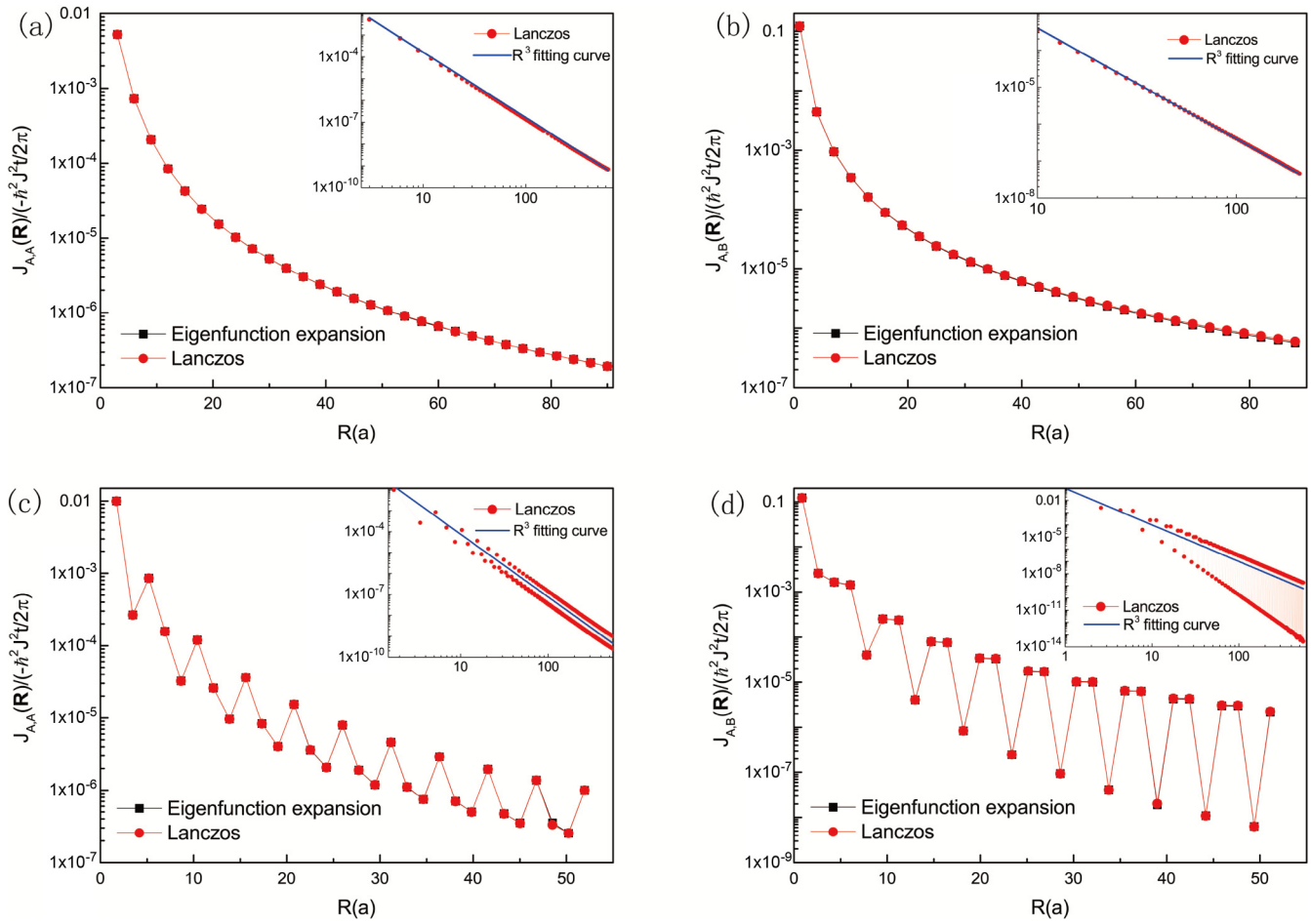

FIG. 2. The RKKY interactions $J_{AA}(\boldsymbol{R})$ along (a) the armchair direction and (c) the zigzag direction and $J_{AB}(\boldsymbol{R})$ along (b) the armchair direction and (d) the zigzag direction in pristine graphene as functions of $R = |\boldsymbol{r}_{lj\alpha} - \boldsymbol{r}_{l'j'\alpha'}|$. The Lanczos method and eigenfunction expansion method yield consistent results, and the insets are the results in main panel replotted in a larger R range in logarithmic scale in order to show clearly the R^{-3} decay law in the large-R limit.

of magnitude, respectively. Note that $J_{BB}(\boldsymbol{R})$ just shows the opposite result due to the inversion symmetry, as mentioned above. Owing to such nontrivial deviations from the RKKY interaction in pristine graphene, in the moderate-R region the R^{-3} decay law breaks down for $J_{\alpha\alpha}(\boldsymbol{R})$'s in the graphene bubble, although it holds true in pristine graphene [see the inset of Fig. 3(a)]. The nontrivial differences of $J_{\alpha\alpha}(\boldsymbol{R})$'s in a graphene bubble from that in pristine graphene arise from the sublattice polarized electronic occupation of the low-energy state around the Dirac point in the graphene bubble. It is well known that in the presence of a uniform magnetic field the $n = 0$ Landau level of a K valley electron in graphene occupies only A sublattices [37]. But this effect is fully compensated by the same Landau level of a K' valley electron. However, under a pseudomagnetic field usually brought about by a strain field, the full sublattice polarization can be realized since the K and K' valley electrons just feel opposite-oriented pseudomagnetic fields. Owing to the lattice deformation, a graphene bubble can also induce a pseudomagnetic field in it, although it is not uniformly distributed in the bubble. Therefore, we speculate that sublattice polarization of the electronic states near the Dirac point (corresponding to the $n = 0$ Landau level) still holds true in the graphene bubble. To verify this argument, we plot the local density of states (LDOS) at two representative lattice points, i.e., $(11, -11, A)$ and $(-11, 11, A)$. As shown in Fig. 3(c), such lattice points are close to $r \approx \pm\sigma$, respectively, and the pseudomagnetic field therein reaches the maximal strength but with opposite sign. From the numerical results shown in Fig. 3(c) we can see that around the Fermi level the LDOS at $(-11, 11, A)$ shows a peak, whereas that at $(11, -11, A)$ shows a gap. Such a result is consistent with the above argument about the sublattice polarized occupation of the low-energy electronic state (in the vicinity of the Dirac point) induced by the pseudomagnetic field. In contrast, as shown in Fig. 3(d), the LDOS spectra at lattice points near the bubble center do not show such a feature. This is due to the fact that the pseudomagnetic field is rather weak near the bubble center; hence, the sublattice polarization of the low-energy states almost disappears therein.

The argument of sublattice polarization of the low-energy states in the strong pseudomagnetic field regions of the bubble can qualitatively account for most features of the RKKY interaction in a graphene bubble shown in Fig. 3(a), in comparison with that in pristine graphene. For example, for $J_{AA}(\boldsymbol{R})$ with the fixed impurity at $(0, 0, A)$, when another impurity occurs in the positive (negative) strong pseudomagnetic field

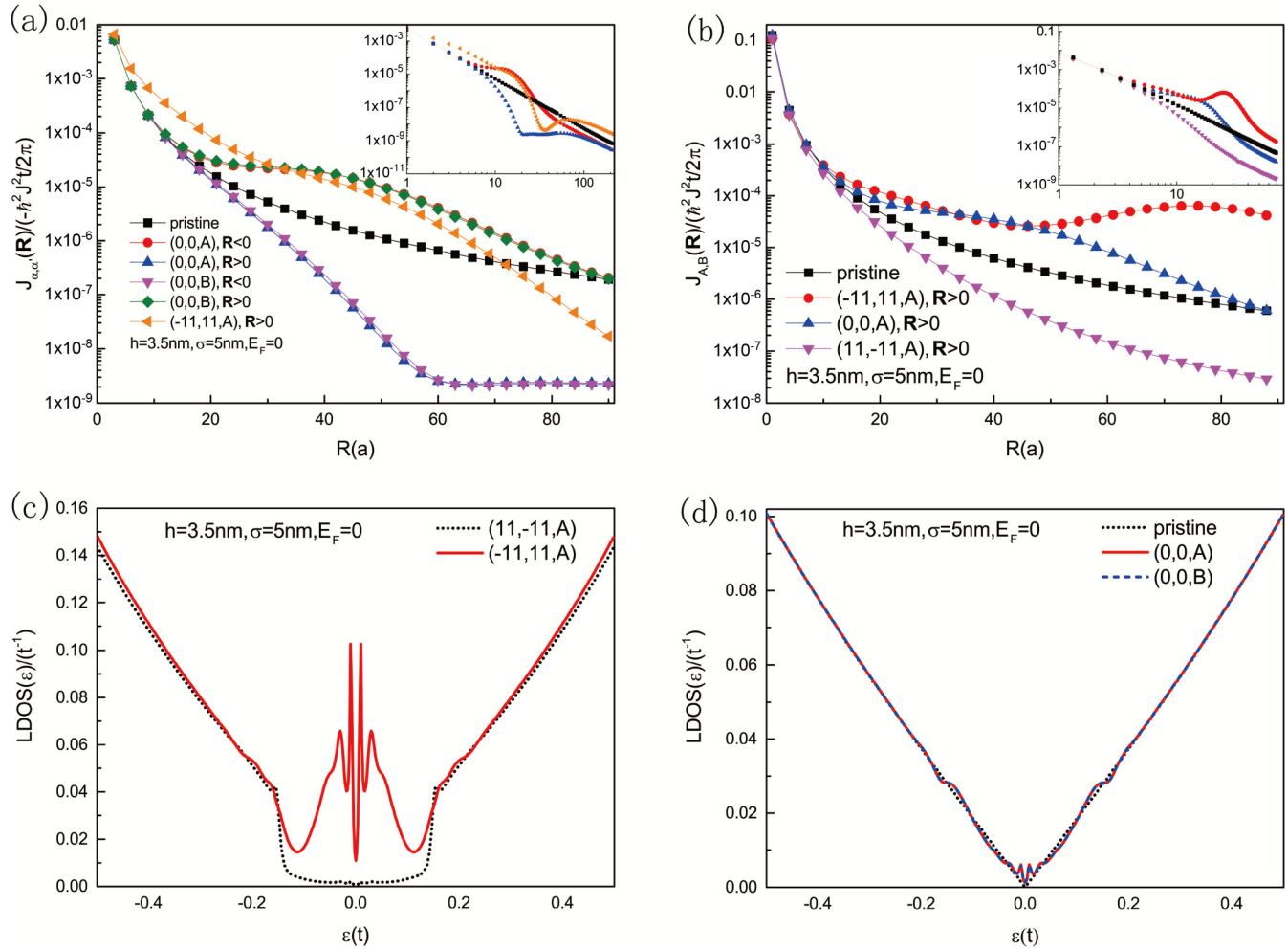

FIG. 3. The RKKY interactions (a) $J_{AA}(\boldsymbol{R})$ and $J_{BB}(\boldsymbol{R})$ and (b) $J_{AB}(\boldsymbol{R})$ along the armchair direction (y axis) in a graphene bubble as functions of $R = |\boldsymbol{r}_{lj\alpha} - \boldsymbol{r}_{l'j'\alpha'}|$. In these results one magnetic impurity is fixed at some typical lattice points specified in the legend. The corresponding result of pristine graphene is also plotted for comparison. The inset replots the results in the main panel in a larger R range in logarithmic scale in order to show clearly the recovery of the R^{-3} decay law in large-R limit. The LDOS spectra at representative lattice points: (c) $(11, -11, A)$ (dotted line) and $(-11, 11, A)$ (solid line) and (d) $(0, 0, A)$ (solid line) and $(0, 0, B)$ (dashed line). In addition, the LDOS of pristine graphene (dotted line) is plotted in (d) for comparison.

regions on the negative (positive) y axis side, the electronic occupations of the lattice points under it are greatly enhanced (reduced) owing to the sublattice polarization of the low-energy states. Notice the RKKY interaction is mainly determined by the low-energy states (around the Fermi level); as a result, it is reasonable that $J_{AA}(\boldsymbol{R} < 0)$ $[J_{AA}(\boldsymbol{R} > 0)]$ is much larger (smaller) than that in pristine graphene.

In Fig. 3(a) the RKKY interaction $J_{AA}(\boldsymbol{R})$ for the case of one impurity is fixed at $(-11, 11, A)$, where the maximal pseudomagnetic field occurs, and is plotted as a function of R as the position of another impurity moves up along the y axis. In comparison with the case of pristine graphene, the electronic states around the Fermi level A-sublattice polarized around the fixed impurity due to the pseudomagnetic field effect. Therefore, it is reasonable that such a $J_{AA}(\boldsymbol{R})$ shown in Fig. 3(a) is larger than its counterpart in pristine graphene when R is not very large. However, with the increase of R, the second impurity enters another maximal pseudomagnetic field region on the positive y-axis side, where A-sublattice occupation is almost forbidden in the electronic states around the Fermi level due to a pseudomagnetic field orientation opposite to that in the region where the first impurity is pinned. As a result, $J_{AA}(\boldsymbol{R})$ decreases with the increase of R. As R increases further, the second impurity exceeds the maximal pseudomagnetic field region on the positive y-axis side, and the suppression of A-sublattice occupation reduces gradually. Therefore, as shown in Fig. 3(a), it is reasonable that the corresponding $J_{AA}(\boldsymbol{R})$ begins to increase. Last but not least, as the second impurity moves out of the bubble $(r > 4\sigma)$, called the large-R region, all the RKKY interactions $J_{\alpha\alpha}(\boldsymbol{R})$ shown in Fig. 3(a) recover the R^{-3} decay rate no matter where the first impurity settles, although the values of these $J_{\alpha\alpha}(\boldsymbol{R})$ in the large-R limit are different from that in pristine graphene.

We now turn to discuss the RKKY interaction in a graphene bubble when two magnetic impurities sit on different sublattice points along the y axis (the armchair direction). In so doing, we consider several typical cases in which the first impurity is fixed at $(0, 0, A)$, $(11, -11, A)$, and $(-11, 11, A)$ respectively. Then $J_{AB}(\boldsymbol{R})$ as a function of R is calculated

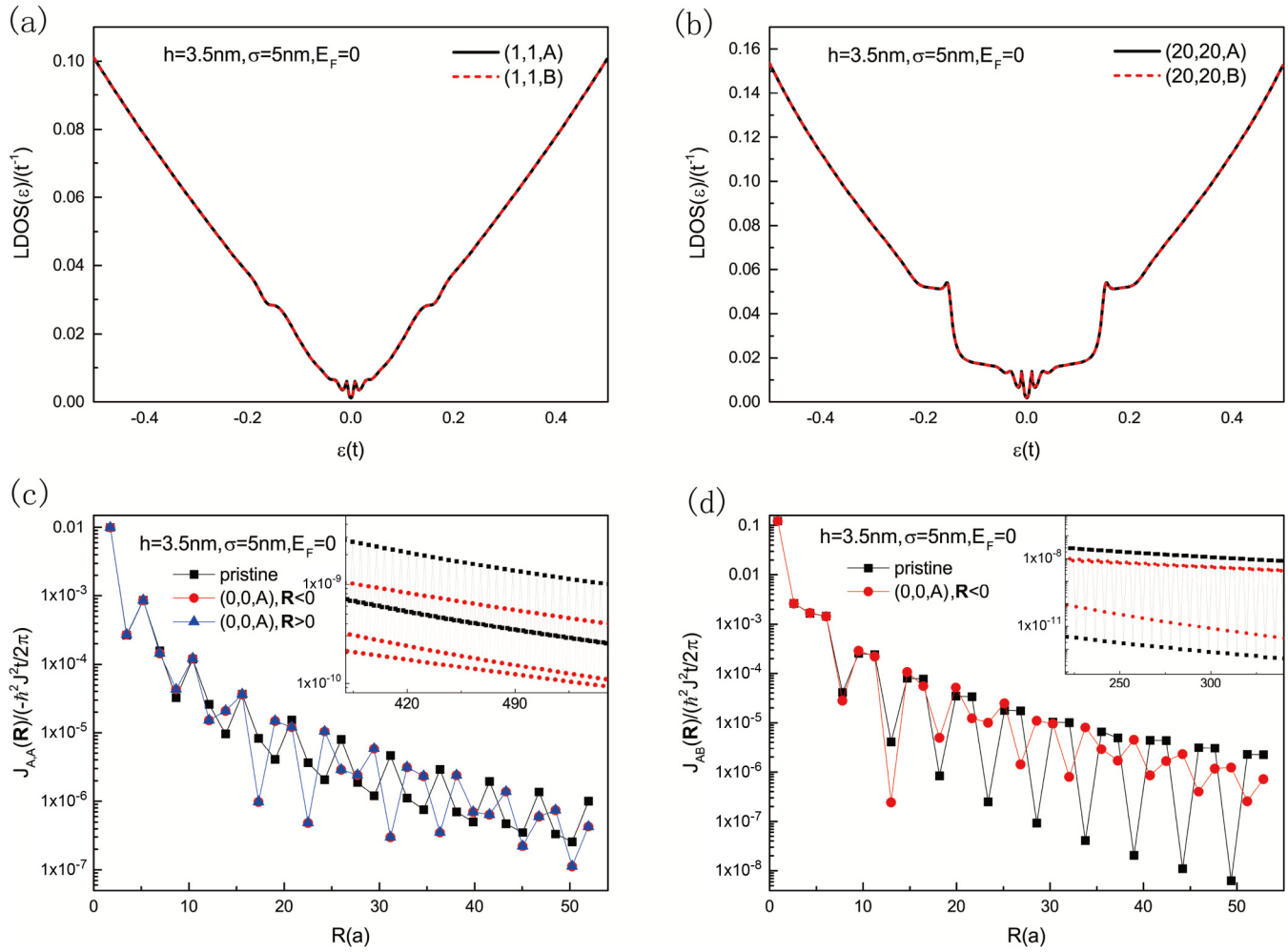

FIG. 4. The LDOS spectra in a graphene bubble at representative lattice points along a zigzag line (a) at $(1, 1, A)$ (solid line) and $(1, 1, B)$ (dashed line) and (b) at $(20, 20, A)$ (solid line) and $(20, 20, B)$ (dashed line). The RKKY interactions (c) $J_{AA}(\boldsymbol{R})$ and (d) $J_{AB}(\boldsymbol{R})$ along a zigzag line in a graphene bubble as functions of $R = |\boldsymbol{r}_{lj\alpha} - \boldsymbol{r}_{l'j'\alpha'}|$. The pinned positions of one magnetic impurity for these results are specified in the legend. The inset replots the results in the main panel in a larger R range in logarithm scale in order to show clearly the recovery of oscillation with a period of three lattice points in the large-R limit.

when the position of the second impurity varies among the B-sublattice points along the y axis. The numerical results are shown in Fig. 3(b). First of all, all of these results for $J_{AB}(\boldsymbol{R})$ are antiferromagnetic, which indicates that the presence of a bubble cannot alter the antiferromagnetic nature of the RKKY interaction between the different sublattices in charge-neutral graphene. In addition, the differences of $J_{AB}(\boldsymbol{R})$'s in the graphene bubble shown in Fig. 3(b) from the corresponding result of the pristine graphene can also be explained by the aforementioned argument about the pseudomagnetic-field-induced sublattice polarization of the low-energy electronic states. For example, as shown in Fig. 3(b), $J_{AB}(\boldsymbol{R})$ for the case in which the first impurity is fixed at $(-11, 11, A)$ is always larger than the result of pristine graphene in the whole R range. Such a result is attributed to the fact that both the A-sublattice points in the pseudomagnetic field region of the negative y-axis side and the B-sublattice points in the pseudomagnetic field region of the positive y-axis side have larger occupation probability in the vicinity of the Fermi level, in comparison with the case of pristine graphene. Finally, when the second impurity occurs outside of the bubble, all kinds of $J_{AB}(\boldsymbol{R})$'s shown in Fig. 3(b) recover the R^{-3} decay rate.

Along a zigzag line across the bubble center, the pseudomagnetic field is very weak everywhere, which can be seen by the calculated LDOS spectra at typical lattice points on such a line. In Figs. 4(a) and 4(b), the LDOS spectra at $(1, 1, A)$ and $(1, 1, B)$, two lattice points near the bubble center, and at $(20, 20, A)$ and $(20, 20, B)$, two lattice points near the half height of the bubble, are plotted, respectively. No notable sublattice polarization can be observed in these LDOS spectra. But these LDOS spectra show, indeed, appreciable differences from that in pristine graphene, in particular, those in the half-height region of the bubble. This reflects the fact that the presence of a bubble can alter the low-energy electronic state a lot. Then, we fix one magnetic impurity at $(0, 0, A)$ to study the RKKY interaction $J_{AA}(\boldsymbol{R})$ as a function of R by altering the position of another impurity along a zigzag line. The numerical result is shown in Fig. 4(c). First, we can see that $J_{AA}(\boldsymbol{R} > \boldsymbol{0})$ and $J_{AA}(\boldsymbol{R} < \boldsymbol{0})$ are identical to each other, which is different from the case of $J_{AA}(\boldsymbol{R})$ along an armchair line, as shown in Fig. 3(a). More importantly, in comparison with the result

of pristine graphene, $J_{AA}(\boldsymbol{R})$ shown in Fig. 4(c) in a graphene bubble does not show a sizable difference by orders of magnitude. This is consistent with the absence of sublattice polarization of the low-energy states along the zigzag line where the pseudomagnetic field is ignorably small. In spite of the absence of a pseudomagnetic field, as shown in Fig. 4(c), $J_{AA}(\boldsymbol{R})$ in a graphene bubble has notable difference from that of pristine graphene along a zigzag line. On the one hand, it oscillates randomly when the two magnetic impurities are both in the bubble region. On the other hand, as seen in the inset of Fig. 4(a), when the second impurity is out of the bubble ($R > 154$), $J_{AA}(\boldsymbol{R})$ oscillates with a period of three lattice points, the same as the result in pristine graphene. However, the former is smaller than the latter on average. This result indicates that the RKKY interaction in a graphene bubble cannot be completely explained in terms of the sublattice polarized electronic occupations under a psuedomagnetic field. As seen from Eq. (5), the RKKY interaction is not completely determined by the projections of the eigenstates onto the specific lattice points. It is also associated with the quantum coherence between the occupied and unoccupied states near the Fermi level. We would like to emphasize that the relationship $J_{AA}(\boldsymbol{R}) = J_{BB}(-\boldsymbol{R})$ is still valid along the zigzag line. Therefore, we need not show the result of $J_{BB}(-\boldsymbol{R})$ in the zigzag direction any more. In addition, the numerical result of $J_{AB}(\boldsymbol{R})$ along the zigzag line is shown in Fig. 4(d). We find that $J_{AB}(\boldsymbol{R})$ does not show a significant difference from $J_{AA}(\boldsymbol{R})$ except that it is antiferromagnetic and it oscillates in phase with the result of pristine graphene in the large-R limit.

According to the above results and discussions, it is more interesting to explore the tunability of the RKKY interaction in a graphene bubble by altering the bubble size or by carrier doping. For such a purpose, we put both magnetic impurities at the maximal pseudomagnetic field regions and choose the lattice points under them to belong to the occupied sublattice. Thus, owing to the sublattice polarization the corresponding RKKY interaction is much larger than that in pristine graphene. More importantly, it is sensitive to the variation of the bubble curvature. In Fig. 5(a) we show the numerical results of $J_{AA}(\boldsymbol{R})$ and $|J_{AB}(\boldsymbol{R})|$ varying with the bubble height h while the bubble width is fixed at $\sigma = 5$ nm. The two magnetic impurities are fixed at $A' = (l, j, \alpha) = (22, 11, A)$ and $A'' = (l', j', \alpha') = (-11, 11, A)$ for $J_{AA}(\boldsymbol{R})$ and $A' = (l, j, \alpha) = (22, 11, A)$ and $B' = (l', j', \alpha') = (11, -11, B)$ for $J_{AB}(\boldsymbol{R})$. As shown in Fig. 1(b), all these points labeled by A', A'', and B' are in the maximal pseudomagnetic field region. We can see that both $J_{A'A''}$ and $J_{A'B'}$ increase with h by more than two orders of magnitude as the maximal h is still a proper value. In Fig. 5(b), we show the numerical results of $J_{A'A''}(\boldsymbol{R})$ and $|J_{A'B'}(\boldsymbol{R})|$ varying with the bubble width σ while the bubble height is fixed at $h = 3.5$ nm. Note that the coordinates of magnetic impurities vary with σ in the case shown in Fig. 5(b). The effect of changing the width of the bubble is similar to that of changing the height of the bubble. As σ increases but h is fixed, the curvature of the bubble decreases. Hence, the strength of the pseudomagnetic field also decreases, which leads to the diminishing of the RKKY interaction strength with the increase of σ. In addition, as discussed above, although the antiferromagnetic coupling of the RKKY interaction between two magnetic impurities at distinct sublattice points is robust in a graphene bubble in the charge-neutral state, if we shift the Fermi level slightly from the Dirac point, which implies carrier doping, we can realize a transition of such a RKKY interaction from antiferromagnetic

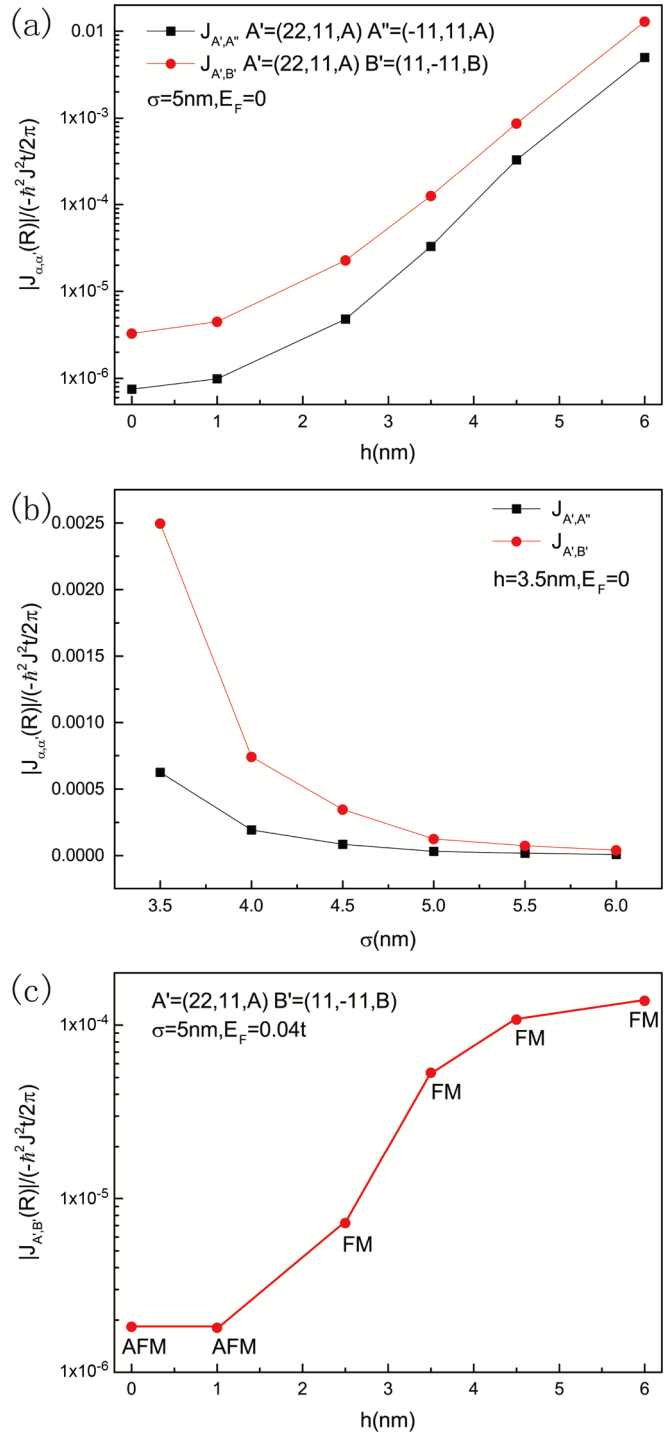

FIG. 5. The RKKY interactions for the magnetic impurities fixed at the typical lattice points A', A'', and B' as labeled in Fig. 1(b). (a) $|J_{\alpha\alpha'}(R)|$ versus h with $\sigma = 5$ nm; (b) $|J_{\alpha\alpha'}(R)|$ versus σ with $h = 3.5$ nm. Note that in (b) the crystal coordinates of magnetic impurities vary with σ as h is fixed. In the cases of (a) and (b) the Fermi level is fixed at $E_F = 0$, but in the case of (c) $E_f = 0.04t$ to account for the carrier doping.

to ferromagnetic coupling by altering the bubble height. Such a numerical result is shown in Fig. 5(c), where $J_{A'B'}$ is shown as a function of h with the Fermi level pinned at $E_F = 0.04t$. We can see that with the increase of the bubble height, $J_{A'B'}$ changes, indeed, from antiferromagnetic to ferromagnetic coupling. Meanwhile, the coupling strength of such a RKKY interaction increases with h considerably. These results shown in Fig. 5 indicate that both the strength and the sign of the RKKY interaction in a graphene bubble can be tuned more conveniently, in contrast to the case in pristine graphene.

IV. CONCLUSIONS

In summary, by means of the Lanczos method, we have performed numerical investigations of the RKKY interaction in a graphene bubble. We have calculated in detail several typical RKKY interactions in a graphene bubble by changing the positions and the interval of two magnetic impurities along both the armchair and zigzag directions. We have found that the RKKY interaction in a graphene bubble can be larger or smaller than the corresponding result in pristine graphene by a few orders of magnitude, depending on the sublattice attribution and pseudomagnetic field strength where two magnetic impurities are positioned, which is due to the sublattice polarization of the low-energy electronic states induced by strong pseudomagnetic field. When the magnetic impurities are both in the bubble region, the R^{-3} decay rate found in pristine graphene breaks down. But it recovers when one magnetic impurity is far away from the bubble center, no matter where another impurity is located. Furthermore, our numerical results indicate that Saremi's rule found in pristine graphene still holds in a charge-neutral graphene bubble. Namely, the RKKY interaction is ferromagnetic if two magnetic impurities are located on the same sublattice; otherwise, it is antiferromagnetic. However, when the Fermi level deviates from the Dirac point by carrier doping, the antiferromagnetic RKKY interaction between two magnetic impurities located on opposite sublattices can be inverted to be ferromagnetic by altering the bubble height. In addition, the strength of the RKKY interaction can be enhanced by more than two orders of magnitude with the increase of the bubble height.

ACKNOWLEDGMENTS

This work was financially supported by the National Natural Science Foundation of China (Grants No. 11474122 and No. 11774123). We thank the High Performance Computing Center of Jilin University for their calculation resources.

[1] P. R. Wallace, Phys. Rev. **71**, 622 (1947).
[2] J. C. Slonczewski and P. R. Weiss, Phys. Rev. **109**, 272 (1958).
[3] Y. Zheng and T. Ando, Phys. Rev. B **65**, 245420 (2002).
[4] K. S. Novoselov, A. K. Geim, S. V. Morozov, D. Jiang, Y. Zhang, S. V. Dubonos, I. V. Grigorieva, and A. A. Firsov, Science **306**, 666 (2004).
[5] K. S. Novoselov, A. K. Geim, S. V. Morozov, D. Jiang, M. I. Katsnelson, I. V. Grigorieva, S. V. Dubonos, and A. A. Firsov, Nature (London) **438**, 197 (2005).
[6] D. A. Abanin, P. A. Lee, and L. S. Levitov, Phys. Rev. Lett. **96**, 176803 (2006).
[7] M. I. Katsnelson, K. S. Novoselov, and A. K. Geim, Nat. Phys. **2**, 620 (2006).
[8] K. S. Novoselov, Z. Jiang, Y. Zhang, S. V. Morozov, H. L. Stormer, U. Zeitler, J. C. Maan, G. S. Boebinger, P. Kim, and A. K. Geim, Science **315**, 1379 (2007).
[9] A. H. Castro Neto, F. Guinea, N. M. R. Peres, K. S. Novoselov, and A. K. Geim, Rev. Mod. Phys. **81**, 109 (2009)
[10] S. Das Sarma, S. Adam, E. H. Hwang, and E. Rossi, Rev. Mod. Phys. **83**, 407 (2011)
[11] M. A. Ruderman and C. Kittel, Phys. Rev. **96**, 99 (1954).
[12] T. Kasuya, Prog. Theor. Phys. **16**, 45 (1956).
[13] K. Yosida, Phys. Rev. **106**, 893 (1957).
[14] V. K. Dugaev, V. I. Litvinov, and J. Barnas, Phys. Rev. B **74**, 224438 (2006).
[15] S. Saremi, Phys. Rev. B **76**, 184430 (2007).
[16] E. Kogan, Phys. Rev. B **84**, 115119 (2011).
[17] M. Sherafati and S. Satpathy, Phys. Rev. B **83**, 165425 (2011).
[18] A. M. Black-Schaffer, Phys. Rev. B **81**, 205416 (2010).
[19] S. R. Power and M. S. Ferreira, Crystals **3**, 49 (2013).
[20] M. A. H. Vozmediano, M. I. Katsnelson, and F. Guinea, Phys. Rep. **496**, 109 (2010).
[21] F. Guinea, M. I. Katsnelson, and A. K. Geim, Nat. Phys. **6**, 30 (2010).
[22] M. Settnes, S. R. Power, J. Lin, D. H. Petersen, and A.-P. Jauho, J. Phys.: Conf. Ser. **647**, 012022 (2015).
[23] M. Neek-Amal and F. M. Peeters, Phys. Rev. B **85**, 195446 (2012).
[24] E. Stolyarova, D. Stolyarov, K. Bolotin, S. Ryu, L. Liu, and K. T. Rim *et al.*, Nano. Lett. **9**, 332 (2009).
[25] T. Georgiou, L. Britnell, P. Blake, R. V. Gorbachev, A. Gholinia, A. K. Geim, C. Casiraghi, and K. S. Novoselov, Appl. Phys. Lett. **99**, 093103 (2011).
[26] N. Levy, S. A. Burke, K. L. Meaker, M. Panlasigui, A. Zettl, F. Guinea, A. H. Castro Neto, and M. F. Crommie, Science **329**, 544 (2010).
[27] V. M. Pereira and A. H. Castro Neto, Phys. Rev. Lett. **103**, 046801 (2009).
[28] M. Settnes, S. R. Power, M. Brandbyge, and A. P. Jauho, Phys. Rev. Lett. **117**, 276801 (2016).
[29] D. Moldovan, M. Ramezani Masir, and F. M. Peeters, Phys. Rev. B **88**, 035446 (2013).
[30] R. Carrillo-Bastos, D. Faria, A. Latgé, F. Mireles, and N. Sandler, Phys. Rev. B **90**, 041411(R) (2014).
[31] V. M. Pereira, A. H. Castro Neto, and N. M. R. Peres, Phys. Rev. B **80**, 045401 (2009).
[32] L. Jiang, X. Lv, W. Gao, G. Yu, Z. Liu, and Y. Zheng, J. Phys.: Condens. Matter **24**, 206003 (2012).
[33] E. Dagotto, Rev. Mod. Phys. **66**, 763 (1994).
[34] C. A. Büsser, G. B. Martins, and A. E. Feiguin, Phys. Rev. B **88**, 245113 (2013).
[35] A. Allerdt, C. A. Büsser, G. B. Martins, and A. E. Feiguin, Phys. Rev. B **91**, 085101 (2015).
[36] C. Lee, X. Wei, J. W. Kysar, and J. Hone, Science **321**, 385 (2008).
[37] M. Koshino and T. Ando, Phys. Rev. B **75**, 033412 (2007).